A Hybrid Symmetric FEM/MOM Formulation applied to Scattering by Inhomogeneous Bodies of Revolution

Daniel J. Hoppe, *Student Member, IEEE*, Larry W. Epp, *Member, IEEE*, and Jin-Fa Lee, *Member IEEE*

Abstract— A new symmetric formulation of the Hybrid Finite Element Method(HFEM) is described which combines elements of the Electric Field Integral Equation (EFIE) and the Magnetic Field Integral Equation (MFIE) for the exterior region along with the finite element solution for the interior problem. The formulation is applied to scattering by inhomogeneous bodies of revolution. To avoid spurious modes in the interior region a combination of vector and nodal based finite elements are used. Integral equations in the exterior region are used to enforce the Sommerfield radiation condition by matching both the tangential electric and magnetic fields between interior and exterior regions. Results from this symmetric formulation as well as formulations based soley on the EFIE or MFIE are compared to exact series solutions and integral equation solutions for a number of examples. The behavior of the symmetric, EFIE, and MFIE solutions is examined at potential resonant frequencies of the interior and exterior regions, demonstrating the advantage of this symmetric formulation.

I. Introduction

Numerical scattering methods have matured from earlier more simple solutions of models for conducting bodies using integral equation methods requiring unknowns only on the surface of the model[Harrington]. Since then necessarily more attention continues to be placed on scattering from inhomogenous objects. The enormous practical uses of dielectric and magnetic materials from substrates and superstrates of microstrip patch antennas to simple uses as impedance matching layers makes this modeling of inhomogenous problems important. Unfortunately present day designers are presented with a multitude of analysis techniques and can still be left with choosing a method based on compromises between modeling accuracy, and the computer demands of run time and memory. Integral equation methods are known to produce highly accurate results, but as the modeling accuracy of inhomogneities is increased they produce a proportionally larger number of unknowns. This hinders the size of the model due to the computer demands. At that time approximate methods of truncating partial differential equation methods may be attractive since local radiation boundary conditions can be applied that maintain the sparsity of these methods. This may alleviate the memory requirements but accuracy can suffer.

So both Integral Equation techniques and partial differential solutions based on the Finite Element Method (FEM) have advantages and disadvantages. Other partial differential approaches such as Finite Difference Time Domain (FDTD) methods exhibit similar problems to the Finite Element Method. In order to accurately model the problem and apply a local boundary condition as an approximation to the Sommerfield Radiation boundary condition, the mesh surrounding the body grows[Mittra]. Recently Lee and Canellaris[Lee] indicate that descretization error increases with the electrical size of the finite element mesh, implying that radiation boundary conditions should be placed close to the body. The mesh size can also grow if the body is irregularly shaped and the applied radiation condition requires a separable surface. Partial differential approaches have the advantage that they are relatively simple to formulate for inhomogenous regions, they avoid the complicated Green's functions of other methods, and they lead to sparse, banded systems.

Many other methods for solving inhomogenous bodies exist[Mei]. But it is the Hybrid Finite Element Method (HFEM) that attempts to merge some of the advantages of both the integral equation methods and the finite element methods[Morgan,Cangellaris,JinHFEM]. With this approach the integral equation mesh used to truncate the interior finite element region can be made conformal to the body. Thus the number of unknowns for the exterior region reverts back to the surface of the body. The sparsity inside the matrix block representing the finite element contribution to the total system remains, reducing the memory demands of the interior region. But since the application of the radiation condition is global in nature, the lower bandwidth of the finite element method is lost when block dense matrices representing the exterior region are placed off the diagonal of the total system matrix.

In most previous HFEM approaches the symmetry present in both the FEM and integral equations methods was also destroyed. Thus the system matrix did not represent a Ritz-Galerkin solution as the domain of the testing functions differs from the domain of the basis set[Strang]. One attempt to retain this symmetry[Jin] requires an apriori matrix inversion before solution of the system matrix. This method has the advantage that multiple right hand sides can the be easily handled.

In hybrid methods tangential electric and magnetic fields on the boundary of the FEM mesh are used to exactly enforce the Sommerfield radiation condition through application of either the Electric Field Integral Equation(EFIE) or the Magnetic Field Integral Equation(MFIE). The method

This work was performed at the Jet Propulsion Laboratory, California Institute of Technology under a contract with the National Aeronautics and Space Administration.

D. J. Hoppe and L. W. Epp are with the Jet Propulsion Laboratory, California Institute of Technology, Pasadena, Ca 91109.

J. F. Lee is with the Worcester Polytechnic Institute, Worcester, MA 01609.

employed here is a simple extension of theses previous methods. By simultaneously using the EFIE and MFIE equations when formulating the hybrid method, continuity of both tangential electric and magnetic fields is uniquely enforced. Unlike previous approches the total system matrix is then symmetric, which leads to computational efficiencies when inverting and eliminates nearly half the unknowns. Also since this formulation exhibits strong non-zero diagonal terms, it lends itself to solution by pre-conditioned iterative methods where only the non-zero elements are stored. When using the Free Space Green's function it is necessary that the interior fields be zero. Since near a resonance this is not the case, erroneous answers result[Yuan] or the resonance can corrupt a decoupled solution[Yuan/Lynch, Cwik]. Recently methods have been proposed to avoid this problem by the introduction of a small amount of free-space loss[Collins], and by incorporation of the Combined Field Integral Equation[Boyse].

The advantages of the symmetric approach described in this paper include those of the previous hybrid approaches. The mesh densities of the internal and external regions can in general be chosen independently, so that the number used per wavelength can be chosen in accordance with previous experience. Here an integer ratio of the nodes of the interior finite element mesh on the boundary to the triangle basis functions used on the exterior boundary for the exterior region provided a simple transition between regions. It will be shown that when enforcing continuity of both tangential fields, the basis set for both the external and interior regions must be chosen correctly or symmetry will be destroyed. The benefit of enforcing both tangential fields will be demonstrated at resonance locations where it alleviates the errors of previous methods and stabilizies the condition number of the system.

II. Problem Description

The problem of scattering by an inhomogeneous body of revolution(BOR) is depicted in Figs. 1-3. As was discussed in the introduction this problem has been considered previously by a number of researchers, including applications of the hybrid finite element method to bodies of revolution and three-dimensional bodies[Jin/Volakis,Yuan,Boyse]. In this particular work a new formulation which results in a symmetric set of equations will be presented. The advantages of such a formulation include a reduction in the storage requirements for the solution of a given problem, the complimentary advantage of the ability to solve larger problems given a specific storage limitation, and a more efficient solution given the existence of specialized solvers for symmetric matrices. In contrast to existing formulations which produce a finite number of zero diagonal terms in the overall impedance matrix the symmetric formulation has dominant, non-zero terms on the diagonal resulting in a more stable matrix solution. The following subsections will discuss the finite element formulation of the internal problem, the integral equation formulation for the external problem, and three methods of combining the interior and exterior formulations to obtain the overall system matrix. The last of these forms is shown to produce a symmetric matrix.

III. Interior Region Finite Element Representation

The internal problem under consideration is depicted in Fig. 2. The interior of the body is assumed to be filled with an inhomogeneous material where the relative permitivity ϵ_r is assumed to be constant throughout the volume, Ω, and the relative permeability, μ_r is a function of both z and the radius ρ, but is independent of the azimuthal angle ϕ. The finite element method is ideally suited for such a problem, and an outline of its application to this specific problem is the subject of the remainder of this subsection.

Since ϵ_r is constant within the interior of the BOR, all components of the electric field are continuous within the volume Ω, and it is convenient to employ the electric field as the unknown field quantity to be determined in the FEM formulation. Maxwell's equations lead to the well known vector wave equation which must be satisfied by the electric field;

$$\nabla \times \left(\frac{1}{\mu_r}\nabla \times \mathbf{E}\right) - k_0^2\epsilon_r\mathbf{E} = 0 \tag{1}$$

The method of weighted residuals may be used to solve the above equation. In this case we demand that

$$\int_\Omega \nabla \left(\times \left(\frac{1}{\mu_r}\nabla \times \mathbf{E}\right) - k_0^2\epsilon_r\mathbf{E}\right) \cdot \mathbf{E}^* d\Omega = 0 \tag{2}$$

where $\mathbf{E}^*$ is an approriately chosen set of testing or weighting functions. Application of the divergence theorem leads to the final form of the FEM equation;

$$\begin{aligned}\int_\Omega \frac{1}{\mu_r}(\nabla \times \mathbf{E}^*) \cdot (\nabla \times \mathbf{E})\, d\Omega \\ - \int_\Omega k_0^2\epsilon_r\mathbf{E}^* \cdot \mathbf{E} d\Omega \\ - j\omega\mu_0 \int_S \mathbf{E}^* \cdot (\hat{\mathbf{n}} \times \mathbf{H})\, dS = 0\end{aligned} \tag{3}$$

This is the first key equation in the development. The functions $\mathbf{E}^*$ are known functions, whereas $\mathbf{E}$, the entire electric field inside the body, as well as $\hat{\mathbf{n}} \times \mathbf{H}$ on the boundary, S, are the unknown quantities to be determined. The detailed expansion of (3) for the axisymmetric BOR case here followed Wilkins et. al.[Wilkins].

IV. Exterior Region Integral Equation Representation

For the external region we examine the equivalent problem depicted in Fig. 3. The BOR is replaced with equivalent currents $\mathbf{J}$ and $\mathbf{M}$ which produce the true field outside

the body and zero field inside the body. When this is the case J and M are related to the true electric and magnetic fields on the boundary S as follows,

$$\mathbf{J} = \hat{\mathbf{n}} \times \mathbf{H} \tag{4}$$

and

$$\mathbf{E} = \hat{\mathbf{n}} \times \mathbf{M} \tag{5}$$

The representation for $\hat{\mathbf{n}} \times \mathbf{H}$ given in (4) may be substituted directly into (3) thereby enforcing continuity of the tangential magnetic field between interior and exterior regions. Note that this substitution will be assumed when referring to equation (3) in the remainder of the text.

Equation (6) links the tangential electric field representations in the interior and exterior regions. It may be tested with an arbitrary set of functions, $\mathbf{J}^*$, generating the second key equation in the development,

$$\int_S \mathbf{J}^* \cdot (\mathbf{E} - \hat{\mathbf{n}} \times \mathbf{M})\, dS = 0 \tag{6}$$

The sources J and M also satisfy the electric field intergral equation, (EFIE), and the magnetic field integral equation, (MFIE). The EFIE is given by,

$$\frac{1}{2}\hat{\mathbf{n}} \times \mathbf{M} = \mathbf{E}^i - L\mathbf{J} + K\mathbf{M} \tag{7}$$

When this equation is tested by $\mathbf{J}^*$ we obtain;

$$\begin{aligned}\int_S \left(-\mathbf{J}^* \cdot K\mathbf{M} + \mathbf{J}^* \cdot \frac{1}{2}\hat{\mathbf{n}} \times \mathbf{M}\right) dS \\ + \int_S \mathbf{J}^* \cdot L\mathbf{J}\, dS \\ = \int_S \mathbf{J}^* \cdot \mathbf{E}^i dS\end{aligned} \tag{8}$$

The operators L and K are described in [Huddleston], and involve the free space Green's function. $\mathbf{E}^i$ is the incident electric field.

Likewise the MFIE is given by,

$$-\frac{1}{2}\hat{\mathbf{n}} \times \mathbf{J} = \mathbf{H}^i - K\mathbf{J} - \frac{1}{\eta_0^2} L\mathbf{M} \tag{9}$$

When the MFIE is tested by a set of arbitrary functions $\mathbf{M}^*$ the fourth key equation in the development is obtained;

$$\begin{aligned}\int_S \left(\mathbf{M}^* \cdot K\mathbf{J} - \mathbf{M}^* \cdot \frac{1}{2}\hat{\mathbf{n}} \times \mathbf{J}\right) dS \\ + \frac{1}{\eta_0^2} \int_s \mathbf{M}^* \cdot L\mathbf{M}\, dS \\ = \int_S \mathbf{M}^* \cdot \mathbf{H}^i dS\end{aligned} \tag{10}$$

Here $\mathbf{H}^i$ is the incident magnetic field, and η_0 is the free space wave impedance.

As discussed in the Appendix, the EFIE, (8), and MFIE, (10), contain redundant information except at specific frequencies where the cavity formed by the exterior surface S becomes resonant. Therefore away from resonance the use of at least one of them along with (6) and (3) provides a unique solution to the scattering problem. In the next subsection three formulations which involve various combinations of (3),(6),(8), and (10) are developed. One of these possible combinations is shown to be symmetric if the expansion and testing functions are chosen appropriately.

V. Three Formulations of the Overall Problem

A. MFIE Formulation

The overall solution requires three vector equations involving E, J and M. The first of these is given by the equation for the interior region (3). Previous researchers have used (6) as a second equation, and (10) as the third equation[Cwik].

With this selection of equations the following system matrix is generated;

$$\begin{bmatrix} Z^{EE} & B^{EJ} & 0 \\ B^{JE} & 0 & G^{JM} \\ 0 & G^{MJ} & G^{MM} \end{bmatrix} \begin{Bmatrix} C^E \\ C^J \\ C^M \end{Bmatrix} = \begin{Bmatrix} 0 \\ 0 \\ V^M \end{Bmatrix} \tag{11}$$

In forming this system (6) and (10) have been scaled by $j\omega\mu_0$, for reasons which will become apparent later in the development. In order to evaluate the matrix entries it is necessary to choose the expansion functions for the unknown quantities E,M, and J.

The nth Fourier component of the electric field in the interior region is expanded as follows;

$$\mathbf{E} = \sum_{i=1}^{N_E} C_t^E(i)\mathbf{e}_t(i)e^{jn\phi} + \sum_{i=1}^{N_N} C_\phi^E(i)\frac{\mathbf{e}_\phi(i)}{\rho}e^{jn\phi} \tag{12}$$

Here $\mathbf{e}_\phi(i)$ is the ith nodal based vector function which is used to expand the ϕ directed component of the electric field, $\mathbf{e}_t(i)$ is the ith edge based vector function which expands the components of the field normal to ϕ. $C_t^E(i)$ and $C_\phi^E(i)$ are the unknown coefficients to be determined. N_N is the number of nodes and N_E is the total number of edges. The expansion functions are defined as

$$\mathbf{e}_t(i) = j(\lambda_{i+1}\nabla_t\lambda_{i+2} - \lambda_{i+2}\nabla_t\lambda_{i+1}) \tag{13}$$

$$\nabla_t = \hat{\rho}\frac{\partial}{\partial\rho} + \hat{\mathbf{z}}\frac{\partial}{\partial z} \tag{14}$$

and

$$\mathbf{e}_\phi(i) = \lambda_i\hat{\phi} \tag{15}$$

where the λ_i are the first-order nodal elements using linear interpolation functions[Silvester].

The unknown currents J and M are expanded as follows,

$$\mathbf{J} = \sum_{i=1}^{N_T} \left(C_t^J(i)\mathbf{j}_t(i) + C_\phi^J(i)\mathbf{j}_\phi(i)\right) e^{jn\phi} \tag{16}$$

and

$$\mathbf{M} = \sum_{i=1}^{N_T} \left(C_t^M(i)\mathbf{m}_t(i) + C_\phi^M(i)\mathbf{m}_\phi(i) \right) e^{jn\phi} \tag{17}$$

The vector expansion functions are defined below;

$$\mathbf{j}_t(i) = \mathbf{m}_t(i) = \hat{\mathbf{t}}\frac{T_i(t)}{\rho(t)} \tag{18}$$

and

$$\mathbf{j}_\phi(i) = \mathbf{m}_\phi(i) = j\hat{\phi}\frac{T_i(t)}{\rho(t)} \tag{19}$$

Here N_T is the number of triangles and $T_i(t)$ is the ith triangle function. As the previous notation suggests, the testing functions are chosen to be the conjugates of the expansion functions in all cases. Substituting the expansions into the appropriate equations the matrix elements may be determined as follows;

$$Z_{\alpha\beta}^{EE}(i,j) = S_{\alpha\beta}(i,j) + T_{\alpha\beta}(i,j) \tag{20}$$

with

$$S_{\alpha\beta}(i,j) = \int_\Omega \frac{1}{\mu_r} (\nabla \times \mathbf{e}_\alpha^*(i)) \cdot (\nabla \times \mathbf{e}_\beta(j))\, d\Omega \tag{21}$$

and

$$T_{\alpha\beta}(i,j) = -\int_\Omega k_0^2 \epsilon_r \mathbf{e}_\alpha^*(i) \cdot \mathbf{e}_\beta(j) d\Omega \tag{22}$$

where α and β are each either t or ϕ.

The terms of the coupling matrices B^{EJ} and B^{JE} are given by the contribution from (3)

$$B_{\alpha\beta}^{EJ}(i,j) = -j\omega\mu_0 \int_S \mathbf{e}_\alpha^*(i) \cdot \mathbf{j}_\beta(j) dS \tag{23}$$

and part of (6)

$$B_{\alpha\beta}^{JE}(i,j) = j\omega\mu_0 \int_S \mathbf{j}_\alpha^*(i) \cdot \mathbf{e}_\beta(j) dS \tag{24}$$

These boundary integrals relate the FEM unknowns representing the tangential fields on the boundary to the tangential fields in the exterior region along with the matrix G^{JM};

$$\begin{aligned} G_{\alpha\beta}^{JM}(i,j) &= -j\omega\mu_0 X_{\alpha\beta}(i,j) \\ &= -j\omega\mu_0 \int_S \mathbf{j}_\alpha^*(i) \cdot (\hat{\mathbf{n}} \times \mathbf{m}_\beta(j))\, dS \end{aligned} \tag{25}$$

The matrices G^{MJ} and G^{MM} may be written in terms of the operator matrices L and K defined in [Huddleston];

$$G_{\alpha\beta}^{MJ}(i,j) = j\omega\mu_0 \left(\frac{\epsilon_{\alpha\beta}}{\eta_0} K_{\alpha\beta}(i,j) - \frac{1}{2} X_{\alpha\beta}(i,j) \right) \tag{26}$$

and

$$G_{\alpha\beta}^{MM}(i,j) = \frac{j\omega\mu_0\epsilon_{\alpha\beta}}{\eta_0^2} L_{\alpha\beta}(i,j) \tag{27}$$

with

$$\epsilon_{\alpha\beta} = \begin{cases} 1 & \text{if } \alpha = \beta = t \\ -1 & \text{if } \alpha = \beta = \phi \\ -j & \text{otherwise} \end{cases} \tag{28}$$

The factors $\epsilon_{\alpha\beta}$ and η_0 appear due to a slight difference in the choice of expansion functions relative to those used in [Huddleston].

The source vector is given by,

$$V_\alpha^M(i) = j\omega\mu_0 \int_S \mathbf{m}_\alpha^*(i) \cdot \mathbf{H}^i dS \tag{29}$$

This completes the formulation based on the MFIE.

B. EFIE Formulation

Since the EFIE and MFIE contain the same information it is also possible to use the EFIE, (8), as the third equation in the formulation. In this case the system matrix has the same form as (11). Only the last equation is modified, with the new entries given by,

$$G_{\alpha\beta}^{MJ}(i,j) = j\omega\mu_0\epsilon_{\alpha\beta} L_{\alpha\beta}(i,j) \tag{30}$$

and

$$G_{\alpha\beta}^{MM}(i,j) = j\omega\mu_0 \left(-\frac{\epsilon_{\alpha\beta}}{\eta_0} K_{\alpha\beta}(i,j) + \frac{1}{2} X_{\alpha\beta}(i,j) \right) \tag{31}$$

and the new source vector is given by,

$$V_\alpha^M(i) = j\omega\mu_0 \int_S \mathbf{m}_\alpha^*(i) \cdot \mathbf{E}^i dS \tag{32}$$

Next a new symmetric formulation of the problem will be described.

C. Symmetric Formulation

The formulations based on the MFIE and EFIE have several undesirable features. The first of these is the fact that a zero matrix lies on the diagonal, leading to an inherently less stable system matrix. Since $G^{JM}(i,j) \neq G^{MJ}(j,i)$ neither of the two formuations is symmetric. In this section a simple symmetric formulation for the problem is deduced.

In the symmetric formulation the first and third equations of the MFIE formulation are retained. The second equation is modified by adding the EFIE to (6). The resulting system has the form,

$$\begin{bmatrix} Z^{EE} & B^{EJ} & 0 \\ B^{JE} & G^{JJ} & G^{JM} \\ 0 & G^{MJ} & G^{MM} \end{bmatrix} \begin{Bmatrix} C^E \\ C^J \\ C^M \end{Bmatrix} = \begin{Bmatrix} 0 \\ V^J \\ V^M \end{Bmatrix} \tag{33}$$

The matrices Z^{EE},B^{EJ},B^{JE},G^{MJ}, and G^{MM}, as well as the source vector V^M are identical to those given in the MFIE formulation. The new second equation now generates the matrices G^{JM} and G^{JJ}, and source vector V^J. Testing the EFIE (8) with $\mathbf{J}^*$ gives the entries of G^{JJ},

$$G_{\alpha\beta}^{JJ}(i,j) = j\omega\mu_0\epsilon_{\alpha\beta} L_{\alpha\beta}(i,j) \tag{34}$$

and adds the additional term to (25)

$$G^{JM}_{\alpha\beta}(i,j) = j\omega\mu_0\left(-\frac{\epsilon_{\alpha\beta}}{\eta_0}K_{\alpha\beta}(i,j) - \frac{1}{2}X_{\alpha\beta}(i,j)\right) \quad (35)$$

and

$$V^J_\alpha(i) = j\omega\mu_0\int_S \mathbf{j}^*_\alpha(i)\cdot\mathbf{E}^i dS \quad (36)$$

Due to the choice of expansion functions for $\mathbf{J}$ and $\mathbf{M}$ the L and X operators are symmetric, whereas the K operator is skew symmetric[Medgyesi-Mitschang]. This guarantees that the G block of the system matrix is symmetric. Since the L and K operators were computed when calculating equations (25) and (26) the additional matrices needed for the symmetric formulation requires little additional computation.

In addition, the Z^{EE} block is easily shown to be symmetric. In order to make the system matrix symmetric coupling matrices B^{JE} and B^{EJ} matrices must satisfy $B^{EJ}(i,j) = B^{JE}(j,i)$. Given the fact that $\mathbf{j}_t(i)$ is pure real and $\mathbf{j}_\phi(i)$ is pure imaginary, this dictates that $\mathbf{e}_t(i)$ must be chosen to be pure imaginary, and $\mathbf{e}_\phi$ must be pure real in order to generate a symmetric system matrix. Similar choices of the finite element basis functions have been used to [Wong, Wilkins PhD] to correctly model the null space of the curl operator to eliminate spurious modes. The above choice of $\mathbf{j}_t(i)$ and $\mathbf{j}_\phi(i)$ can be found from similar reasoning due to their relationship to the total tangential electric fields on the boundary.

The next section will present a few examples of results generated using each of the three formulations discussed above.

VI. Results

A. The Dielectric Sphere

The first example considered is plane wave scattering from a dielectric sphere where $\epsilon_r = 2.0$. The finite element mesh for this problem is shown in Fig. 2. This same mesh will be used for sweeping through a fairly wide range of frequencies. Therefore the mesh density was chosen so that there would be ≈ 10 triangle basis functions on the dielectric boundary per wavelength in the dielectric at the highest frequency of interest($f = 82.80$ GHz), requiring 41 boundary nodes. Using a 2 to 1 ratio of triangles to edges on the boundary to transition into the interior region gave ≈ 33 nodes per wavelength and ≈ 57 edges per wavelength in the model at the highest frequency of interest. Therefore more than sufficient samples were taken per wavelength at the lower frequencies. The matrix order for the $n = 0$ harmonic is 1020, consisting of 239 unknown nodal values, 705 edge values and 19 triangle basis functions in the exterior giving an additional 76 unknowns. For harmonics where $n \neq 0$, the matrix order was 1006. The difference is accounted for by elimination of the unknown edge values on the axis of symmetry which are zero for the basis functions chosen.

Figs. 4 and 5 show the computed results for the three separate formulations for the $\phi\phi$ and $\theta\theta$ bistatic RCS. The sphere is excited by an incident plane wave from $\theta = 180.0°$ and $\phi = 0.0°$ requiring solution of the $n = \pm 1$ harmonics. It should be noted that in general it is not necessary to recalculate the elements of (33) for a negative index such as $n = -1$ after their computation for $n = +1$. For the computations shown here these properties were exploited for the more computationally intensive blocks of G and V. For Figs. 4 and 5 the frequency is chosen such that $ka = 1.0$ giving $a = 1.5916$ mm for $f = 30$ GHz. For comparison, the Mie series expansion of the sphere was used. For later condition number comparison all three cases were solved using a full matrix LU decomposition. The symmetric formulation was also solved using a iterative conjugate gradient algorithm based on Lanczos algorithm[Golub and Van Loan]. This symmetric solver stores only the 8,653 non-zero elements above and on the diagonal of the matrix. The numerical integrals used in computing the matrix elements for the exterior region were computed by gaussian quadrature.

The interior resonance location for the dielectric-filled sphere can be found at $k_d a = 2.744$ where k_d propagation constant in the dielectric, $\epsilon_r = 2.0$. Tangential edge elements were used to help eliminate spurious FEM solutions. And because the solution did not require inversion of the matrix Z^{EE} as done by other authors[Jin,Cwik] no instabilities where introduced at interior resonant frequencies. The results at the interior resonant frequency are shown in Figs. 6 and 7.

B. The Dielectric Sphere at an Exterior Resonance

A second resonance, referred to as the exterior resonance here, occurs when the interior of the body is replaced with free space. This resonance is associated with the application of the integral equations in the external region. It is necessary to examine the solution in a finite region around the analytical resonant location of a sphere, $k_0 a = 2.744$, to account for modeling effects introduced by the segmented approximation to the boundary. To understand the numerical stability and uniqueness of the solution in this region the estimate of the condition number of the three solutions was examined, Fig. 8. The condition number for the EFIE, MFIE, and symmetric fromulations was computed for the mesh density as previously discussed, and shown in Fig. 2, which contains 41 boundary nodes. In addition Fig. 8 also gives the condition number estimate for the symmetric formulation with an increased mesh density using 61 boundary nodes which will be discussed later.

The condition number estimate is taken from the inverse of the minimum pivot element. The solution to the EFIE and MFIE formulations is corrupted due to the onset of this resonance. By running closely spaced frequency points, every 25 MHz, Fig. 8 shows that at there is a location, $f = 82.80$ GHz, where the resonance causes a jump in the condition number of the symmetric formulation. The results in Figs. 9 and 10 show that the symmetric formulation also

is slightly corrupted at this location. As discussed in the Appendix, from a purely analytical standpoint this corruption is unexpected and must be due to numerical inaccuracy. In order to show this the number of basis functions on the boundary will now be increased and the calculation repeated.

As mentioned previously, Fig. 8 also gives the condition number for the symmetric formulation using 61 boundary nodes. This increases the number of basis functions on the external boundary from 10 per wavelength in the dielectric to 15. It was found that condtion number of this system, when sampled every 25 MHz, did not exhibit as large of a condition number jump. The maximum condition number occurred at f = 82.25 GHz where the results are shown in Figs. 11 and 12. The symmetric formulation gives good agreement and again the EFIE and MFIE are corrupted. The symmetric formulation guarantees the continuity of the tangential electric and magnetic fields as discussed in the Appendix. Therefore increasing the number of basis functions on the boundary more explicitly enforces this continuity. This is more important at resonance where the contamination due to the resonant currents can be present. Thus for this example it was possible to remove the resonance problem simply by increasing the sampling density on the outer boundary.

Note that in general the condition number(with 41 boundary nodes) of the symmetric formulation is one to two orders of magnitude less than those of the other formulations. This can be explained in part by the dominance of the diagonal terms in the symmetric formulation and by the preconditioning scheme used. Since all the diagonal elements of the symmetric formulation are non-zero, it was found that a simple preconditioning that normalized all the diagaonal elements to unity magnitude was sufficient although others are possible[Golub and Van Loan]. In order to reduce the condition number of the EFIE formulation, it was found necessary to scale the last equation of the EFIE formulation by $1/\eta_0$.

C. The Dielectric Cylinder

To further explore the numerical stability of these formulations a dielectric cylinder, $\epsilon_r = 2.0$, a = 2.707 mm was used. The first exterior resonance of this cylinder occurs at f = 42.7 GHz. Using 69 boundary nodes gives 15 triangle basis functions per wavelength in the dielectric at this frequency. The matrix order for the $n \neq 0$ modes was 1388 which consisted of 326 nodal, 930 edge and 132 triangle basis function unknowns. Fig. 13 gives the esimate of the condition number for the three solutions. The condition number estimates exhibit the same behavior as shown in Fig. 8, with a small jump in the symmetric formulation with the maximum occurring at f = 42.85 GHz. Figs. 14 and 15 show the calculated RCS of these solutions compared to an integral equation solution encorporating the PMCHW formulation[Huddleston] at f = 42.85 GHz. The segementation of the boundary was identical for all solutions.

VII. Conclusions

A symmetric formulation for scattering by inhomogeneous bodies of revolution has been presented. The symmetric formulation reduces the storage requirments, and allows for the use of symmetric, iterative, sparse matrix solvers. The resulting symmetric system matrix is compared to that obtained using a simple EFIE or MFIE formulation. Several examples have been given to illustrate the accuracy of all three formulations as well as their stability at the resonant frequencies of the body. The symmetric formulation has also been shown to reduce numerical inaccuracy due to exterior resonances.

Appendix
Behavior of the Formulations at Exterior Resonances

In this appendix we consider the behavior of the EFIE, MFIE, and symmetric formulations at frequencies where the cavity formed by the exterior surface of the BOR, filled with free space, is resonant. In order to guarantee a unique solution to the scattering problem the interior and exterior representations for the tangential electric and magnetic fields must be equal on the boundary S. In this appendix it will be shown that this condition is not met by either the EFIE or MFIE formulations but is met by the symmetric formulation.

Consider first of all the EFIE formulation. In this case in the exterior problem the tangential electric field is forced equal to zero just inside the boundary of the body. This implies that equation (6) does indeed guarantee that the tangential electric fields from the interior and exterior regions match. This can be shown by substituting the definition for $\mathbf{M}$ into equation (5),

$$\mathbf{E} = \hat{\mathbf{n}} \times \mathbf{M} = \hat{\mathbf{n}} \times \hat{\mathbf{n}} \times \left(\mathbf{E}^- - \mathbf{E}^+\right) \tag{37}$$

where $\mathbf{E}$ represents the electric field from the finite element representation and $\mathbf{E}^+$ and $\mathbf{E}^-$ are the electric fields just inside (−) and just outside (+) S. The EFIE forces $\mathbf{E}^- = 0$ and the previous equation gives,

$$\mathbf{E} = \mathbf{E}^+ \tag{38}$$

as required. It can be shown that when there is no exterior resonance, forcing the tangential electric field just inside the body also forces the tangential magnetic field equal to zero[Yaghjian]. However, at a resonance the tangential magnetic field is not forced to zero, and may be equal to an undetermined amount of resonant mode current[Yaghjian]. Thus when the EFIE is used at resonance we have,

$$\mathbf{J} = \hat{\mathbf{n}} \times \left(\mathbf{H}^+ - \mathbf{H}^-\right) = \hat{\mathbf{n}} \times \mathbf{H}^+ - \alpha \mathbf{J}_{\mathbf{res}} \tag{39}$$

where $\alpha \mathbf{J}_{res}$ is the unknown quantity of resonant mode current. Substituting this relationship into equation (4) reveals that at resonance the interior and exterior magnetic fields may differ by an undetermined quantity of this mode

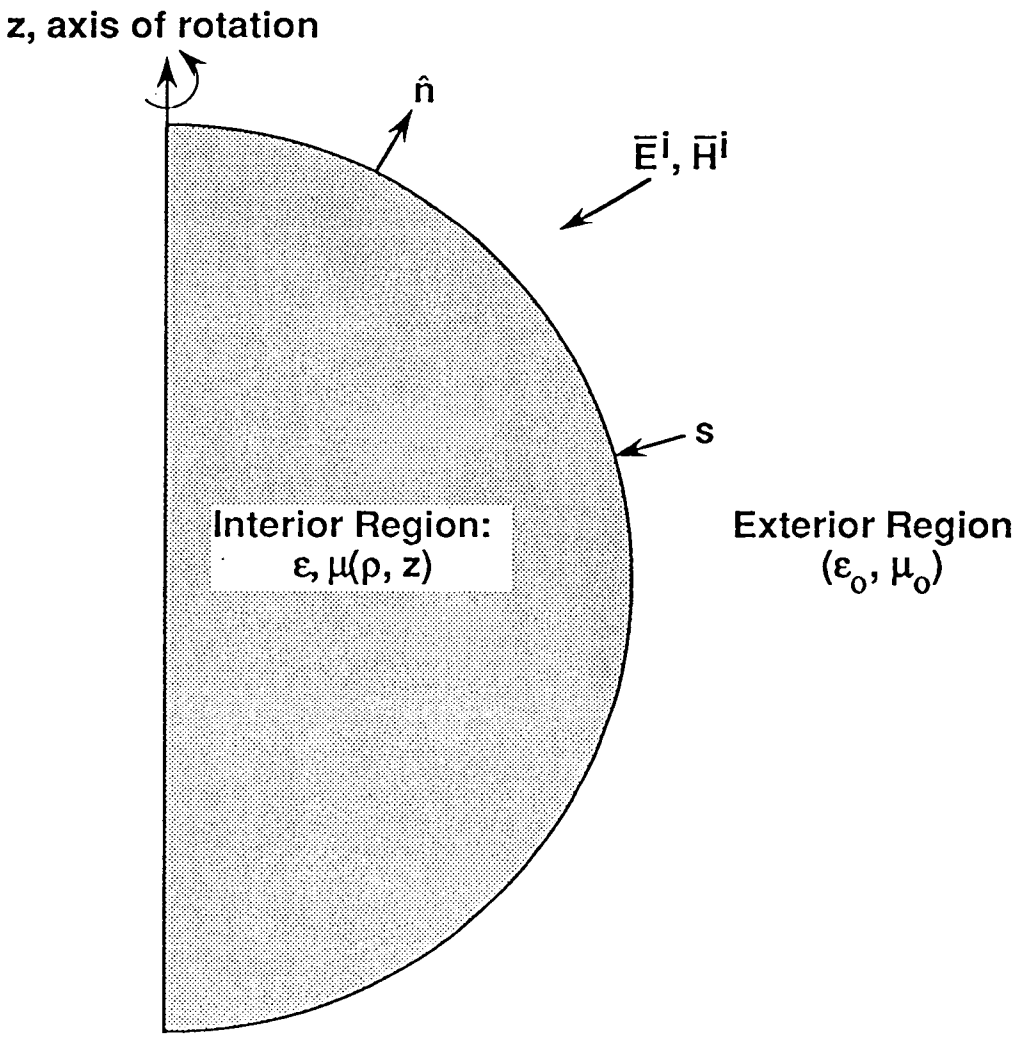

Fig. 1. Original Problem: Scattering due to an inhomogeneous body

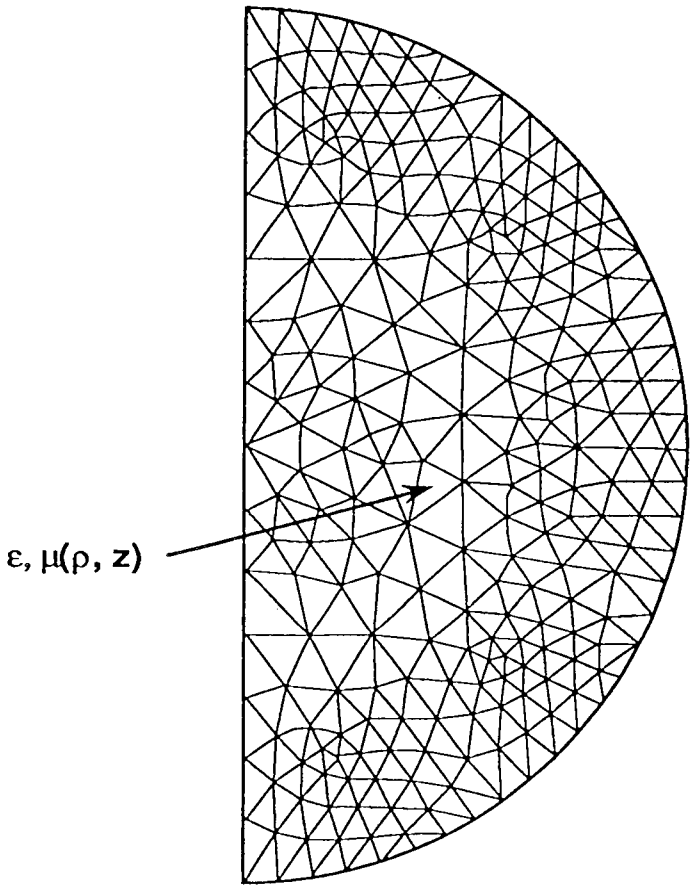

Fig. 2. Equivalent problem for the interior region showing finite element mesh

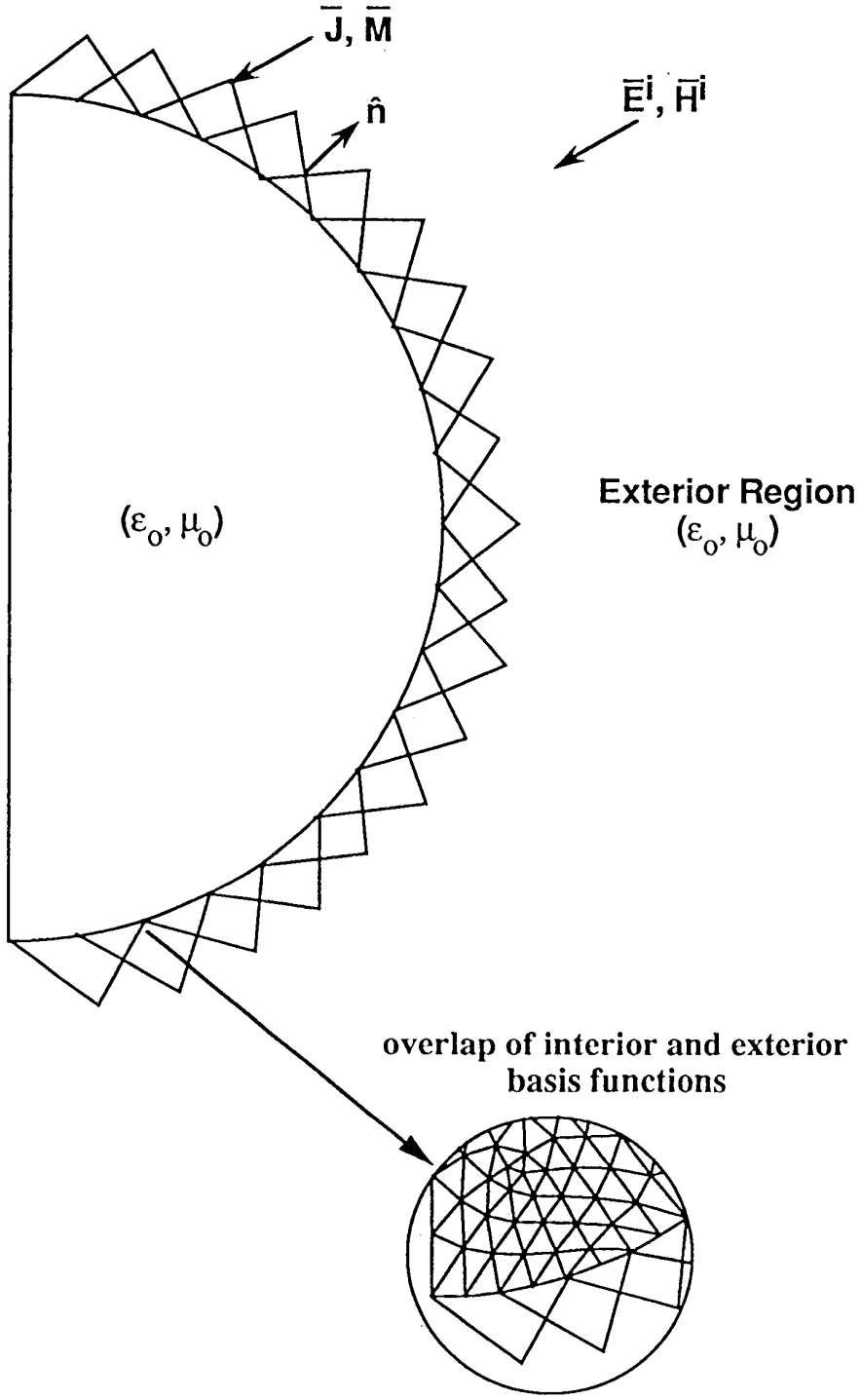

Fig. 3. Equivalent problem for exterior region

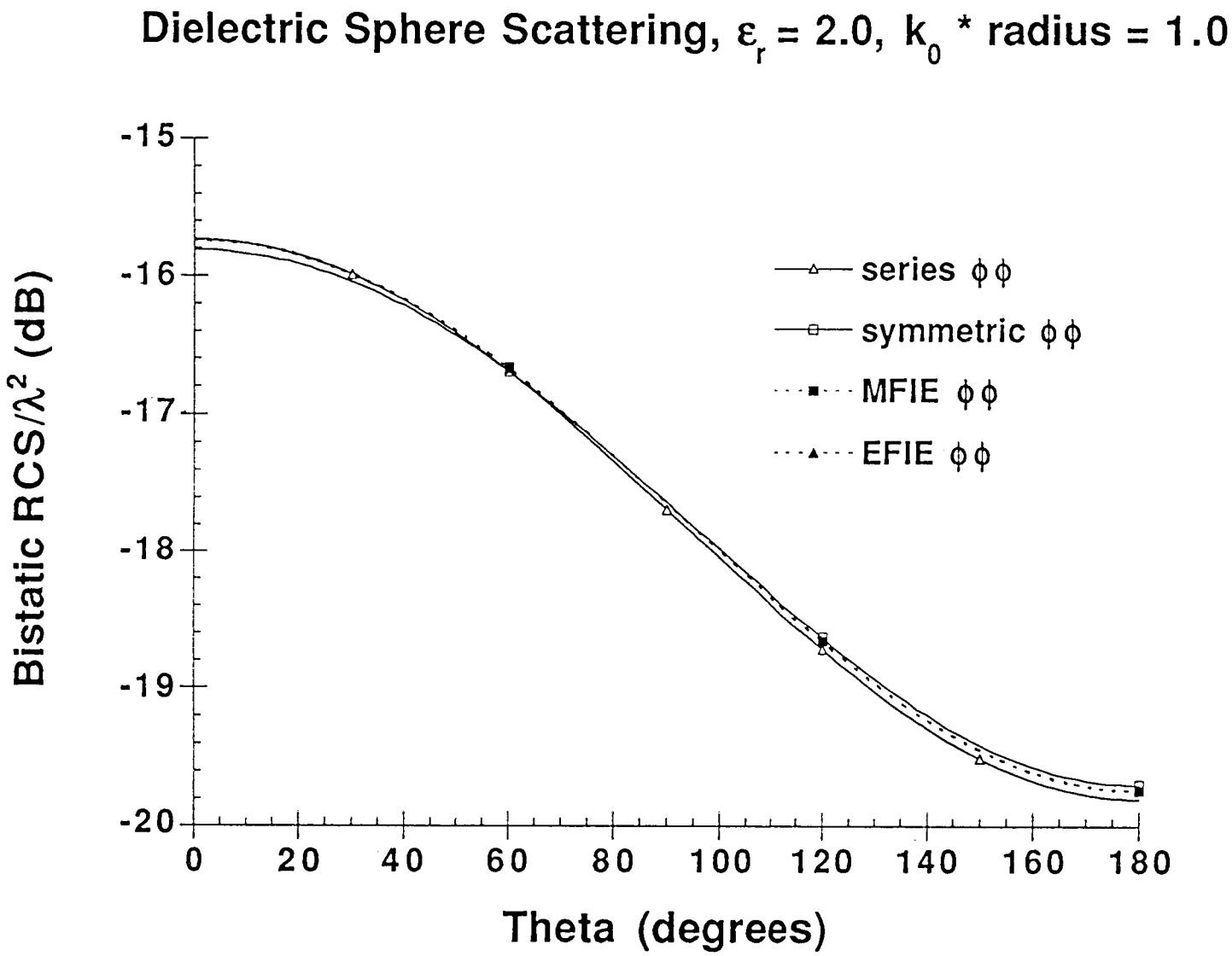
Dielectric Sphere Scattering, ε_r = 2.0, k_0 * radius = 1.0
Bistatic RCS/λ^2 (dB)
-15
-16
-17
-18
-19
-20
0
20
40
60
80
100
120
140
160
180
Theta (degrees)
series $\phi\phi$
symmetric $\phi\phi$
MFIE $\phi\phi$
EFIE $\phi\phi$

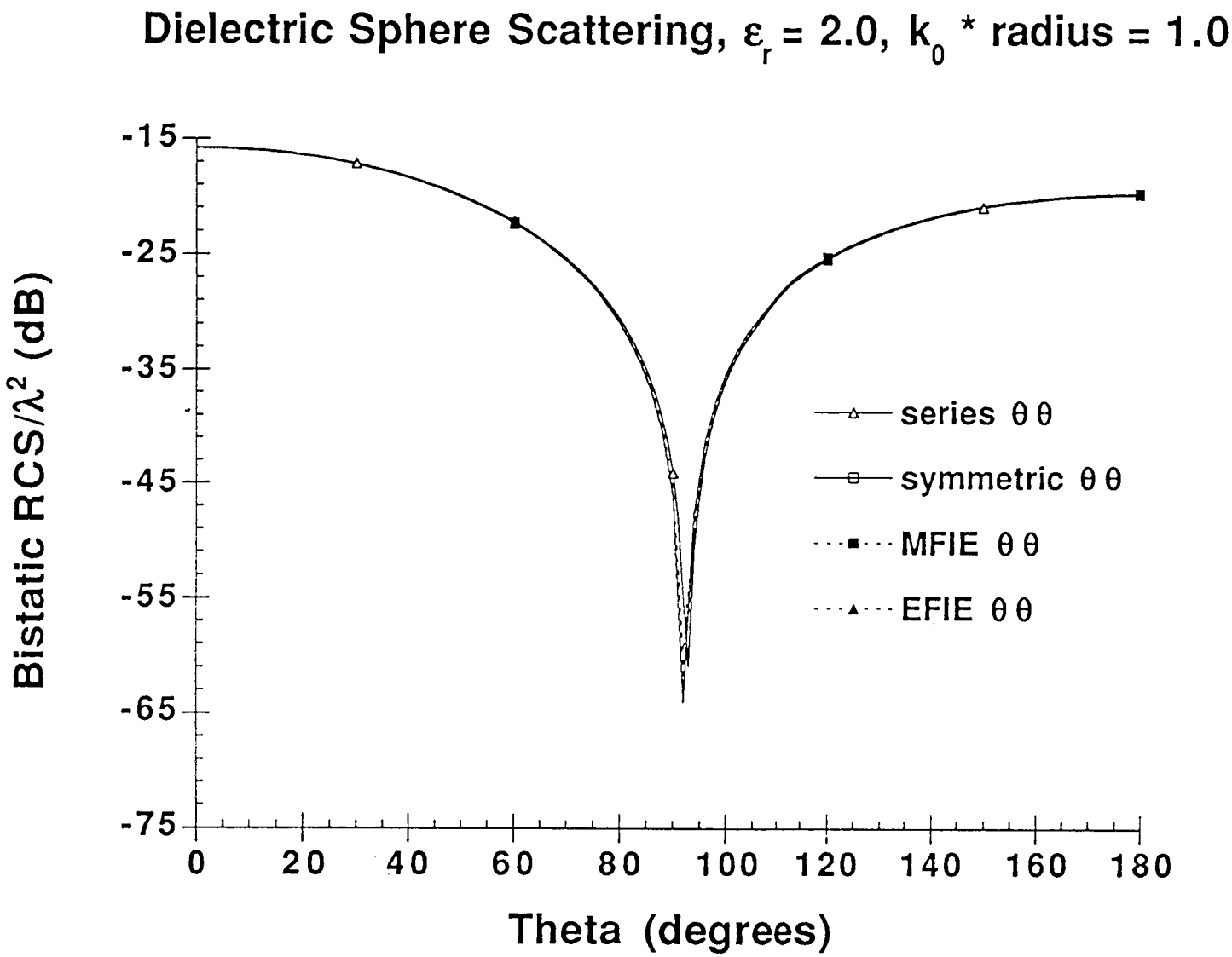
Dielectric Sphere Scattering, ε_r = 2.0, k_0 * radius = 1.0
Bistatic RCS/λ^2 (dB)
-15
-25
-35
-45
-55
-65
-75
0
20
40
60
80
100
120
140
160
180
Theta (degrees)
series θθ
symmetric θθ
MFIE θθ
EFIE θθ

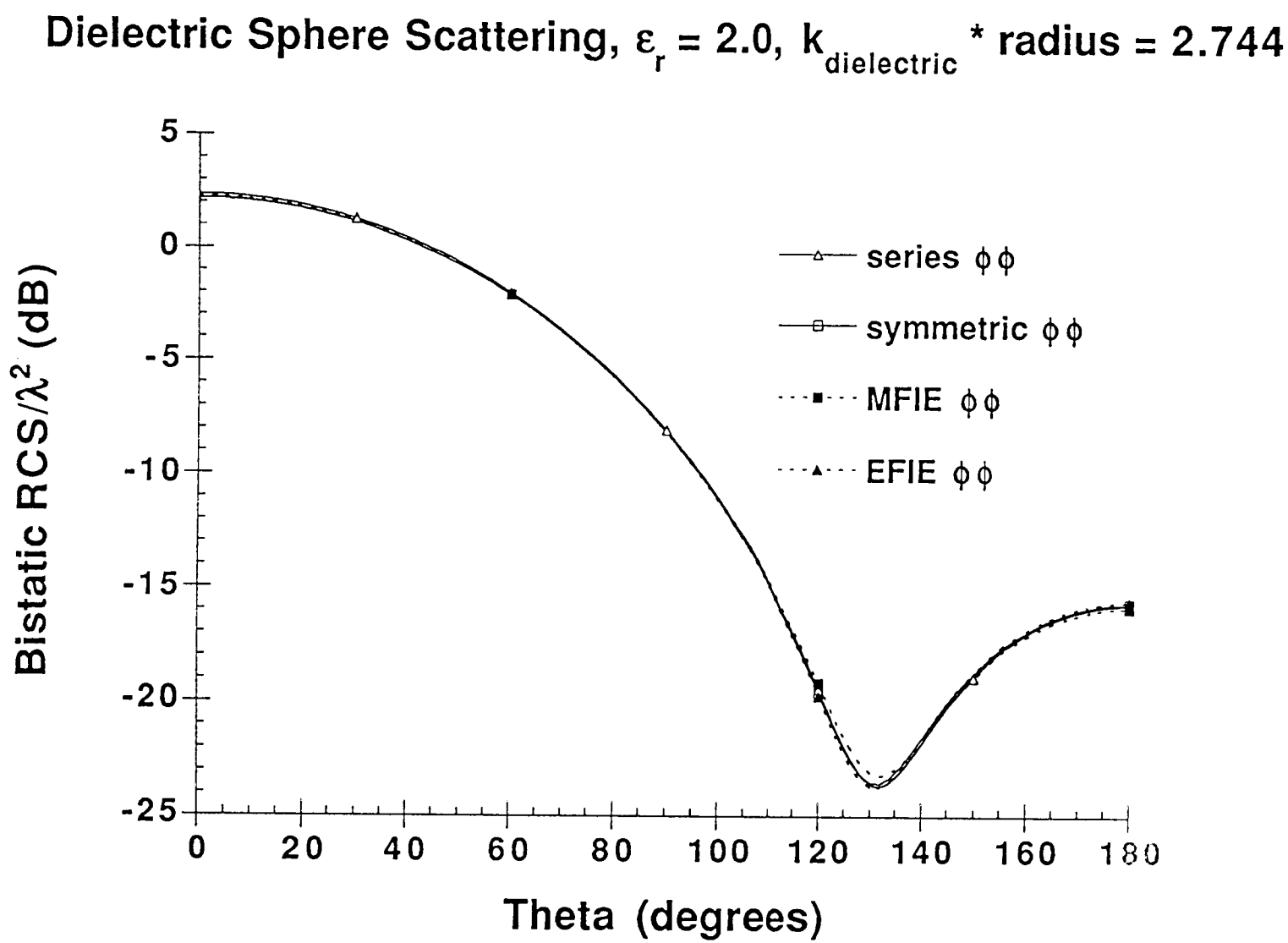
Dielectric Sphere Scattering, ε_r = 2.0, $k_{dielectric}$ * radius = 2.744
Bistatic RCS/λ^2 (dB)
5
0
-5
-10
-15
-20
-25
0
20
40
60
80
100
120
140
160
180
Theta (degrees)
series $\phi\phi$
symmetric $\phi\phi$
MFIE $\phi\phi$
EFIE $\phi\phi$

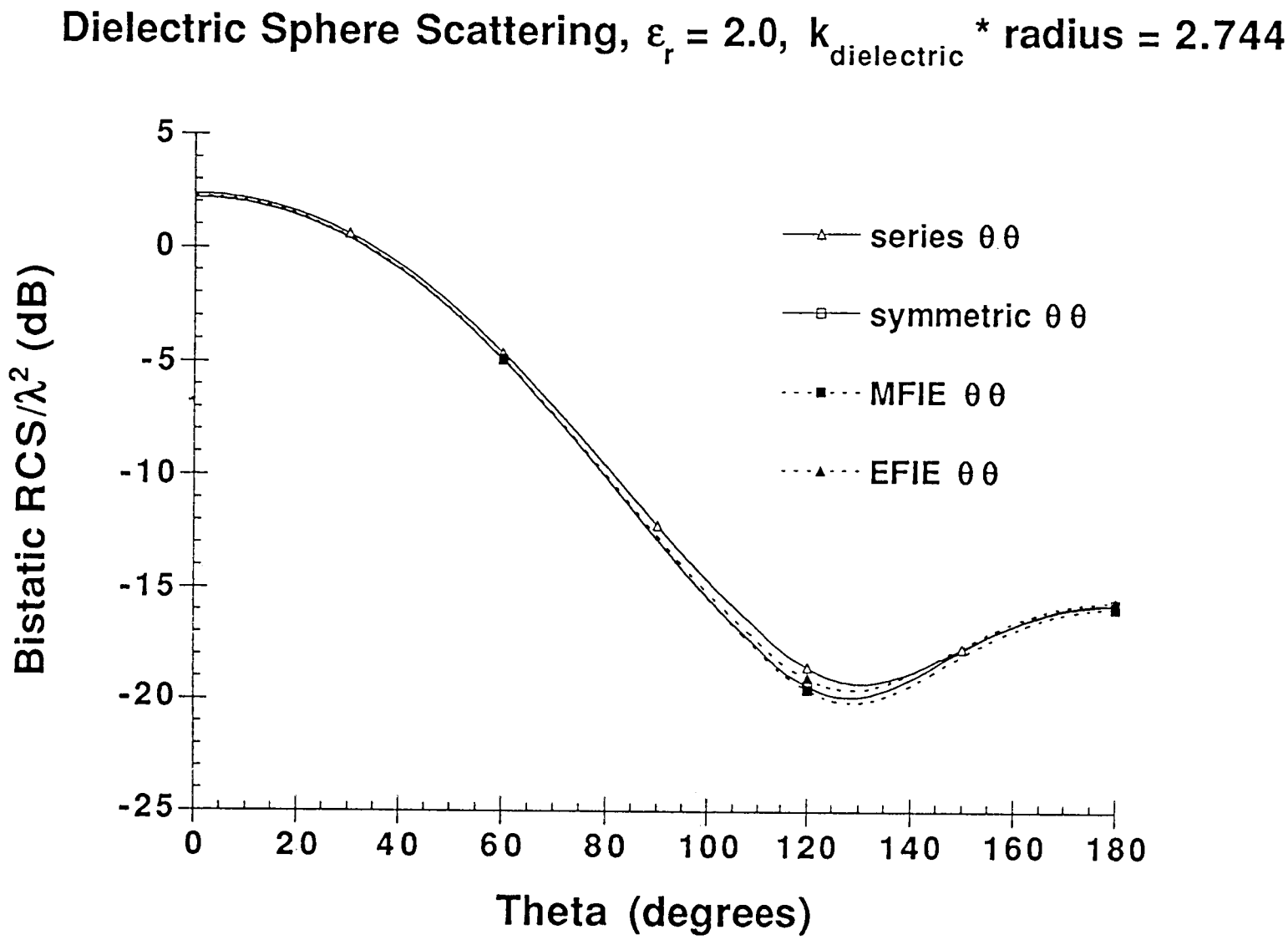
Dielectric Sphere Scattering, ε_r = 2.0, $k_{dielectric}$ * radius = 2.744
Bistatic RCS/λ^2 (dB)
5
0
-5
-10
-15
-20
-25
0
20
40
60
80
100
120
140
160
180
Theta (degrees)
series θθ
symmetric θθ
MFIE θθ
EFIE θθ

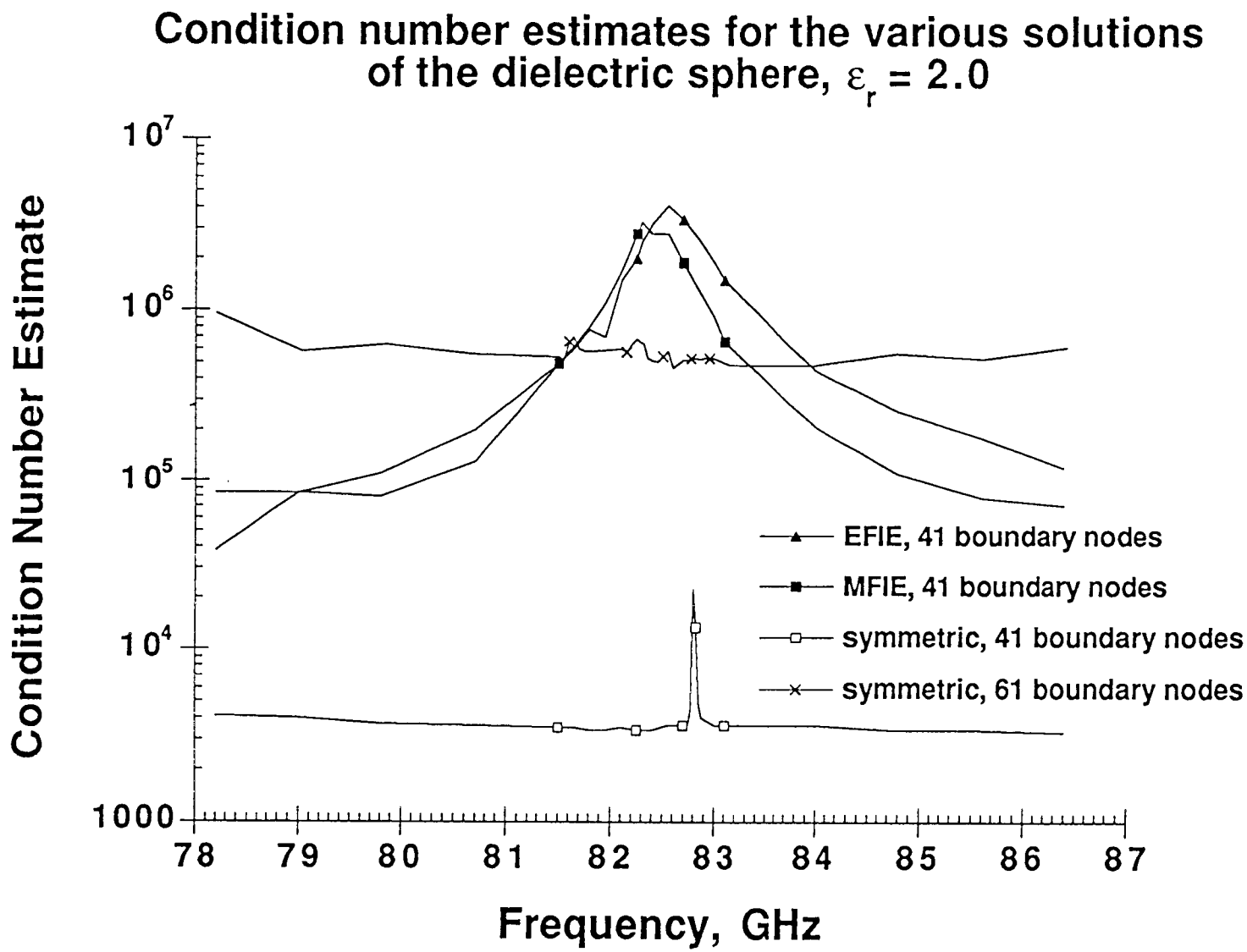
Condition number estimates for the various solutions of the dielectric sphere, $\varepsilon_r = 2.0$
Condition Number Estimate
10^7
10^6
10^5
10^4
1000
78
79
80
81
82
83
84
85
86
87
Frequency, GHz
EFIE, 41 boundary nodes
MFIE, 41 boundary nodes
symmetric, 41 boundary nodes
symmetric, 61 boundary nodes

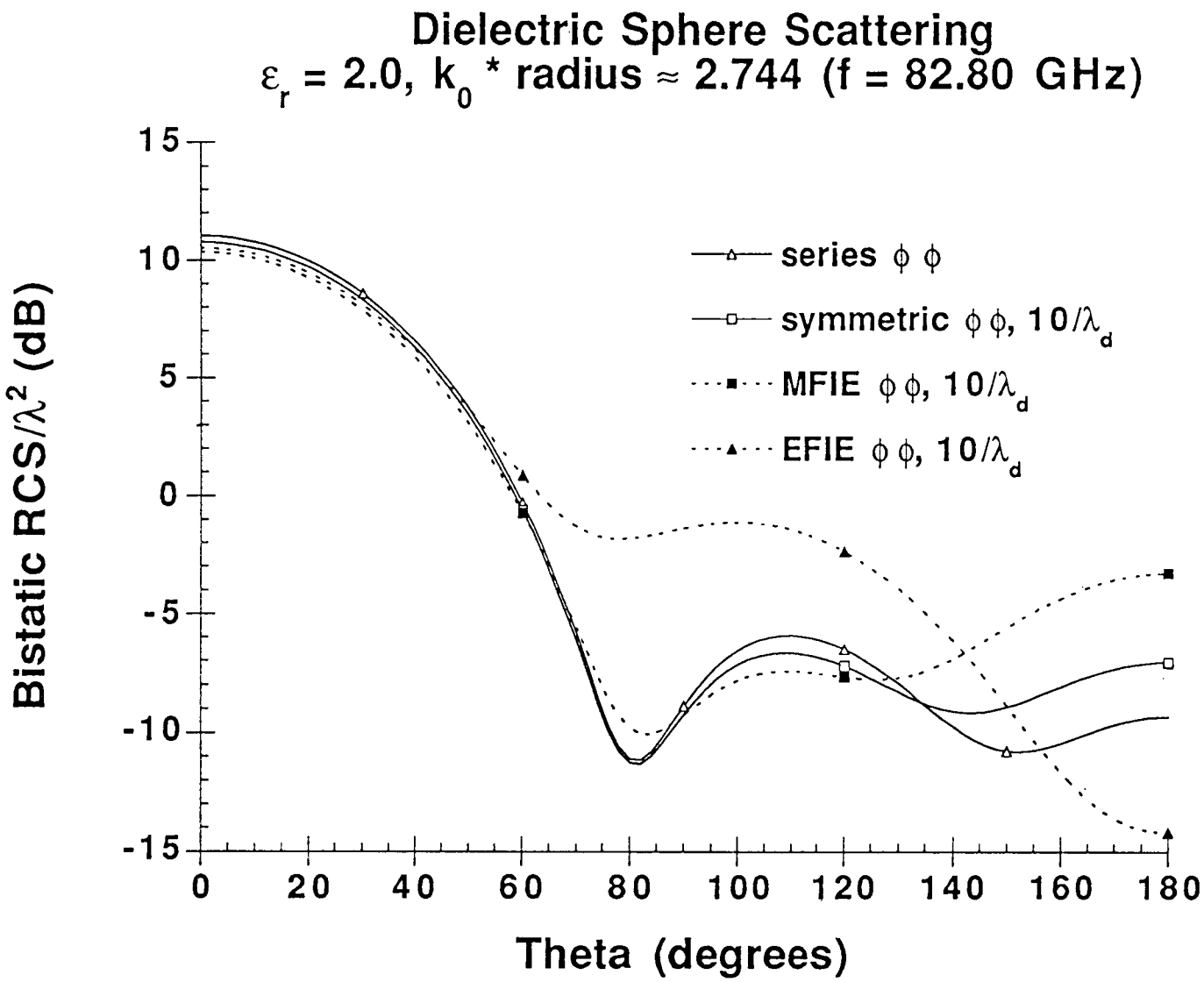
Dielectric Sphere Scattering
ε_r = 2.0, k_0 * radius ≈ 2.744 (f = 82.80 GHz)
Bistatic RCS/λ^2 (dB)
15
10
5
0
-5
-10
-15
0
20
40
60
80
100
120
140
160
180
Theta (degrees)
series $\phi\,\phi$
symmetric $\phi\,\phi$, 10/λ_d
MFIE $\phi\,\phi$, 10/λ_d
EFIE $\phi\,\phi$, 10/λ_d

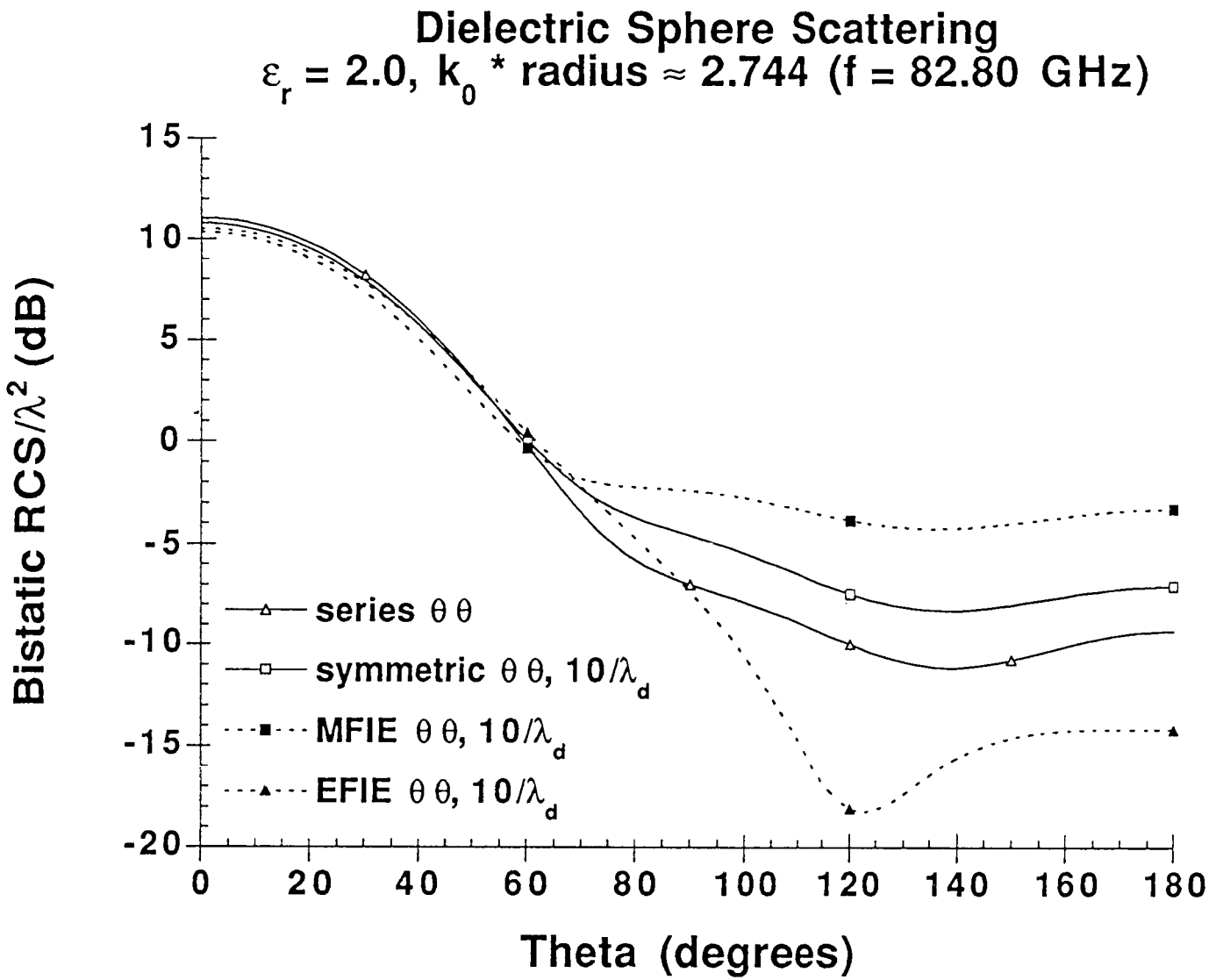
Dielectric Sphere Scattering
ε_r = 2.0, k_0 * radius ≈ 2.744 (f = 82.80 GHz)
Bistatic RCS/λ^2 (dB)
15
10
5
0
-5
-10
-15
-20
0
20
40
60
80
100
120
140
160
180
Theta (degrees)
series θ θ
symmetric θ θ, 10/λ_d
MFIE θ θ, 10/λ_d
EFIE θ θ, 10/λ_d

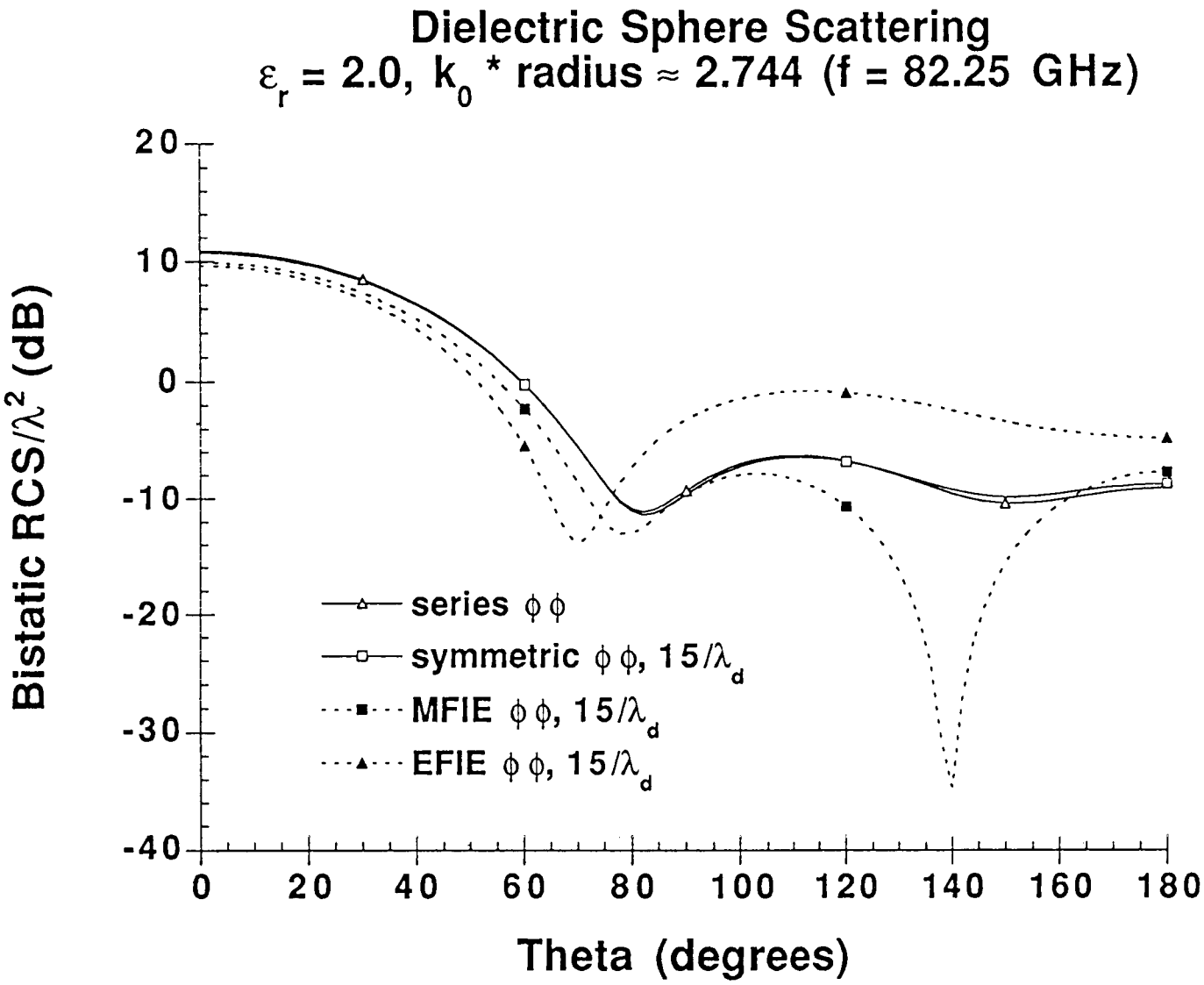
Dielectric Sphere Scattering
ε_r = 2.0, k_0 * radius ≈ 2.744 (f = 82.25 GHz)
Bistatic RCS/λ^2 (dB)
20
10
0
-10
-20
-30
-40
0
20
40
60
80
100
120
140
160
180
Theta (degrees)
series $\phi\phi$
symmetric $\phi\phi$, 15/λ_d
MFIE $\phi\phi$, 15/λ_d
EFIE $\phi\phi$, 15/λ_d

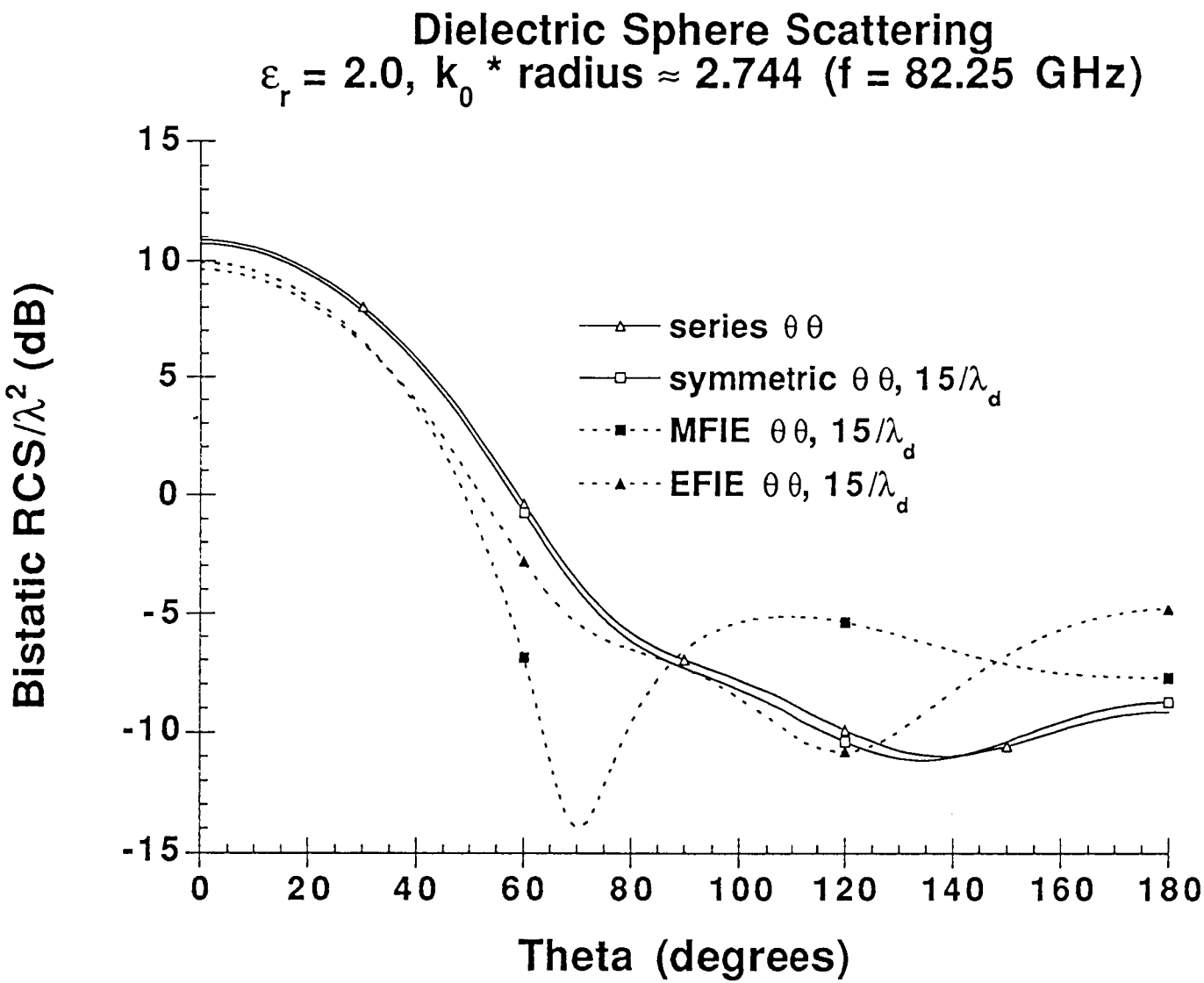
Dielectric Sphere Scattering
ε_r = 2.0, k_0 * radius ≈ 2.744 (f = 82.25 GHz)
Bistatic RCS/λ^2 (dB)
15
10
5
0
-5
-10
-15
0
20
40
60
80
100
120
140
160
180
Theta (degrees)
series θ θ
symmetric θ θ, 15/λ_d
MFIE θ θ, 15/λ_d
EFIE θ θ, 15/λ_d

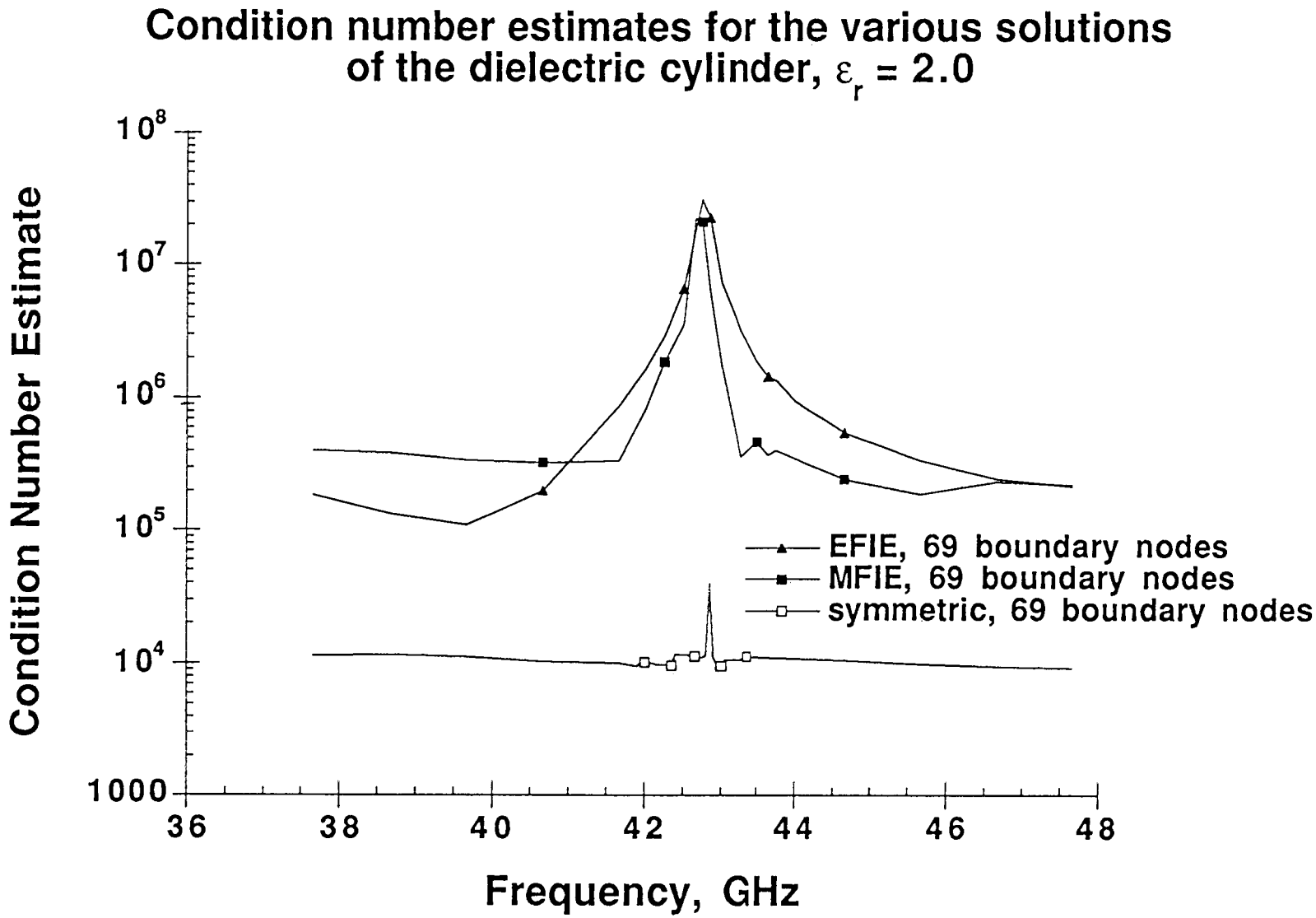
Condition number estimates for the various solutions
of the dielectric cylinder, ε_r = 2.0
Condition Number Estimate
10^8
10^7
10^6
10^5
10^4
1000
36
38
40
42
44
46
48
Frequency, GHz
EFIE, 69 boundary nodes
MFIE, 69 boundary nodes
symmetric, 69 boundary nodes

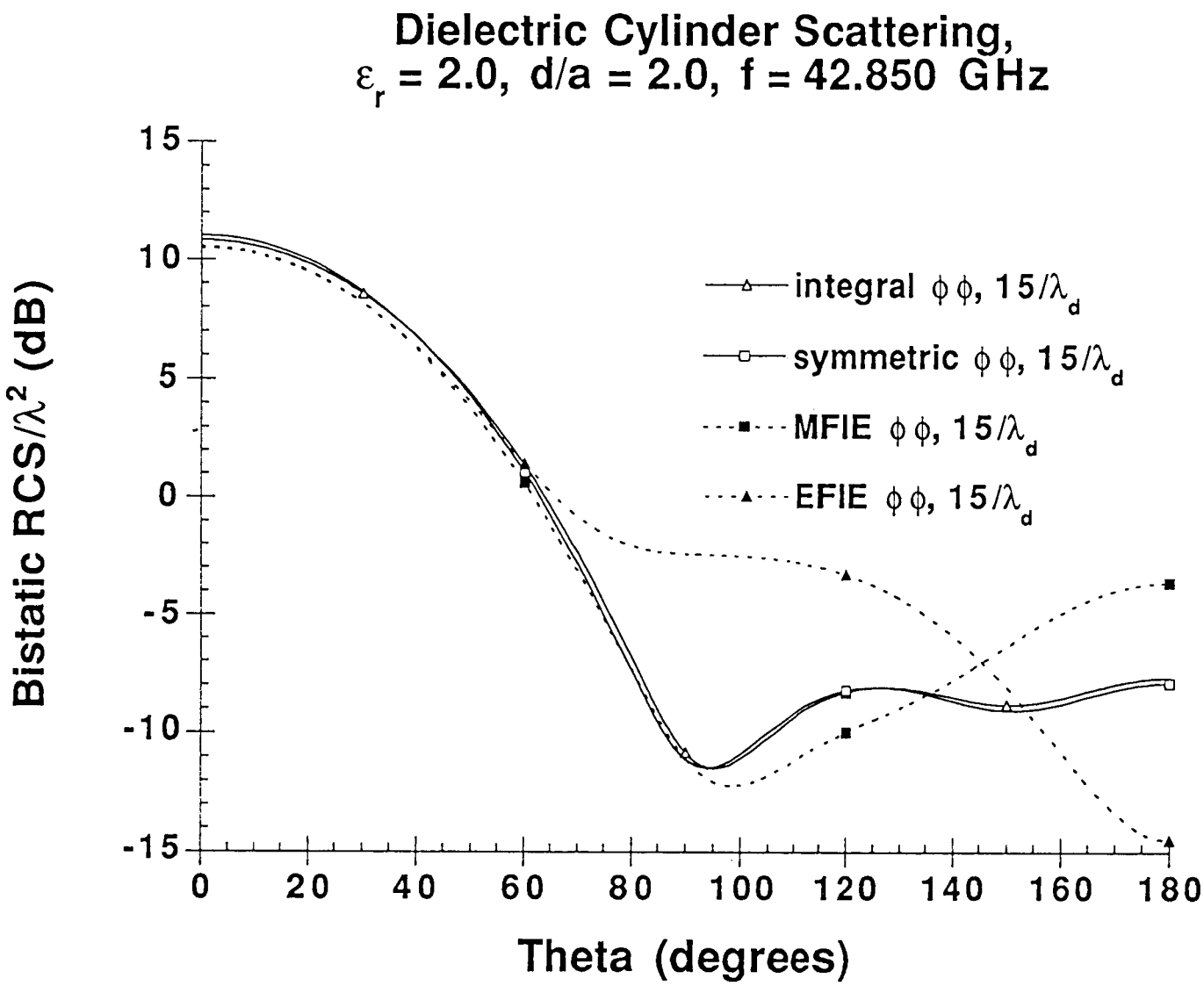
Dielectric Cylinder Scattering,
ε_r = 2.0, d/a = 2.0, f = 42.850 GHz
Bistatic RCS/λ^2 (dB)
15
10
5
0
-5
-10
-15
0
20
40
60
80
100
120
140
160
180
Theta (degrees)
integral $\phi\phi$, 15/λ_d
symmetric $\phi\phi$, 15/λ_d
MFIE $\phi\phi$, 15/λ_d
EFIE $\phi\phi$, 15/λ_d

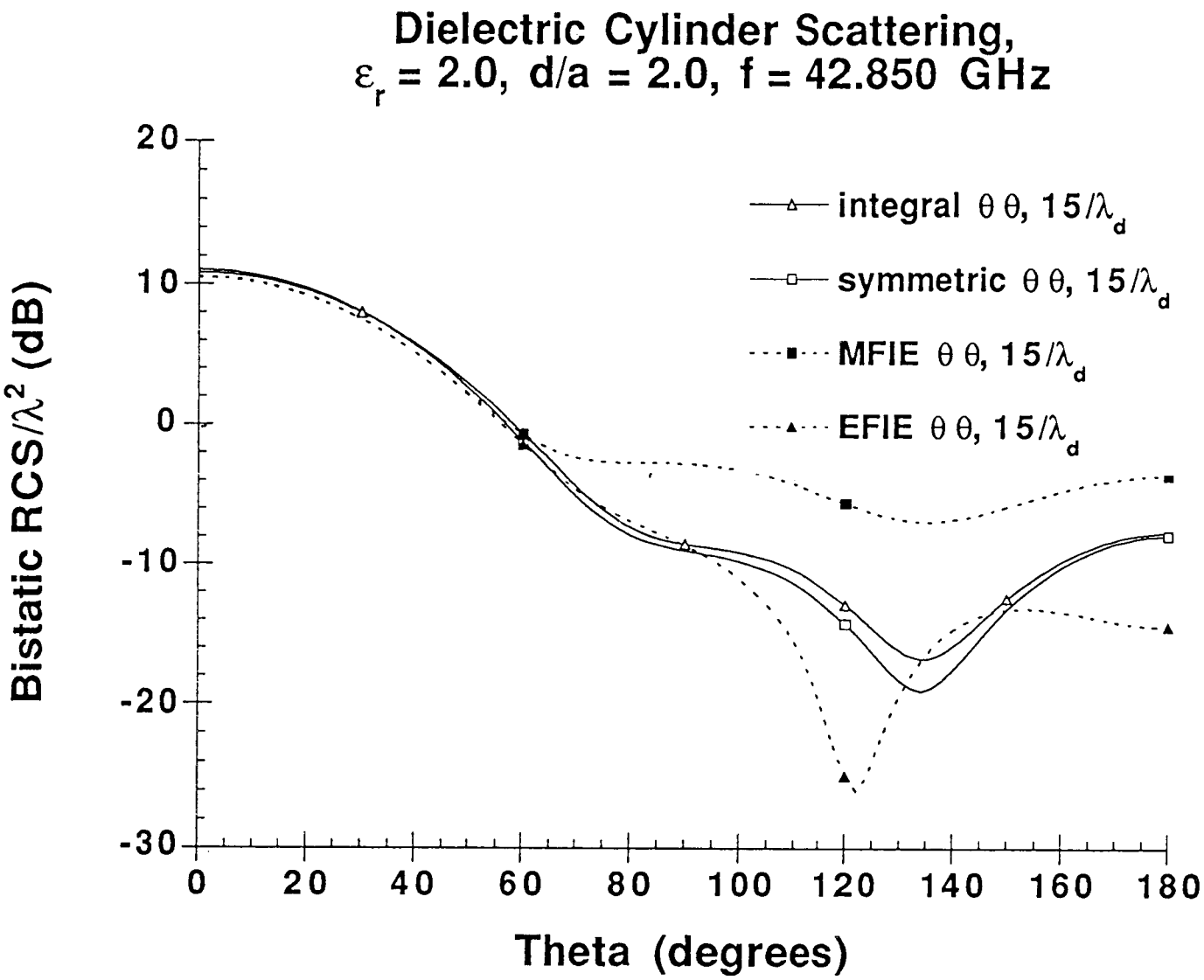
Dielectric Cylinder Scattering,
ε_r = 2.0, d/a = 2.0, f = 42.850 GHz
integral θ θ, 15/λ_d
symmetric θ θ, 15/λ_d
MFIE θ θ, 15/λ_d
EFIE θ θ, 15/λ_d
Bistatic RCS/λ^2 (dB)
20
10
0
-10
-20
-30
0
20
40
60
80
100
120
140
160
180
Theta (degrees)